Plasmonic effect on quantum coherence and interference in metallic photonic crystals doped with quantum dots

Ali Hatef and Mahi R. Singh

Department of Physics and Astronomy, The University of Western Ontario, 1151 Richmond Street, London, Ontario N6 A 3K7, Canada

(Received 8 March 2010; published 21 June 2010)

We have studied the effect of plasma energy on the absorption coefficient of metallic photonic crystals doped with an ensemble of three-level quantum dots, which are interacting with each other via dipole-dipole interaction. The quantum dots are also interacting with coupled plasma-photon modes present in the system. A probe laser field is applied in order to study the absorption coefficient. We also consider the effect of quantum interference in our simulations, whereby two absorbed photons interfere with one another. Here the density matrix method has been used to calculate the steady-state and transient behavior of the absorption coefficient for the system. Two different field configurations are considered in our numerical simulations. In the first configuration, a probe field couples the ground state and two closely excited states. Absorption occurs due to transitions from the ground state to the two excited states. It is found that the position of the transparent peak moves when the plasma energy is changed. In other words, changing the plasma energy causes the system to switch between a transparent and an absorbing state. The strong coupling between plasmons and the quantum dots is responsible for this phenomenon. In the second configuration, the probe field couples with only one excited state, while a pump field couples to the other excited state. The transition between excited states is dipole forbidden. We observed that the peak in the absorption profile splits into two and also that the system exhibits gain with inversion due to the change in the plasma frequency, which is caused by quantum interference and coherence. These are interesting results and can be used make nanoscale plasma devices.

DOI: 10.1103/PhysRevA.81.063816 PACS number(s): 42.50.Gy

I. INTRODUCTION

The aim of the present work is to study the quantum optics of metallic photonic crystals (MPCs) doped with an ensemble of quantum dots (QDs), while considering the dipole-dipole interaction (DDI). Recently, intensive experimental and theoretical research has been done on MPCs and metallo-dielectric photonic crystals because of their ability to control electronic and photonic resonances simultaneously [1–8]. Photonic crystals made from metallic nanolayers or spheres are more reflective than those made of dielectric or semiconductor materials over a broader range of frequencies. Therefore, these nanoscale metal-based structures are more likely to possess a complete photonic band gap (PBG) than their dielectric counterparts. Furthermore, this PBG will be effective for crystals with fewer lattice periods, even if the total thickness of metal in the MPC is hundreds of skin depths in length [1]. The PBG that formed by a MPC is the result of a combination of plasma screening effects and Bragg scattering.

In dielectric photonic crystals, high dielectric contrast is required to have a complete PBG. For example, inverse opal photonic crystals require this contrast to be over a factor of 8 to get a PBG in the optical regime [2]. In terms of fabrication, this restriction causes a great deal of difficulty. Materials with energy dependent dielectric constants, such as metals, are the best alternative to overcome this barrier. On the other hand, photons interact much more strongly with metals than dielectrics, making MPCs more useful for developing integrated photonic devices. Devices may be designed with fewer lattice constants, making elements simpler to fabricate and easier to pack densely. MPCs also have many applications in the field of telecommunications, as antennas, all-optical switches, biosensors, and solar cells.

Initially, studies on MPCs were focused within the range of microwave and far-infrared frequencies, owing to the fact that the metallic layers are strong reflectors in the range of these frequencies [3]. However, due to the improvement in microfabrication techniques, several samples of MPCs that operate in the visible or near-infrared frequency range have been fabricated. These MPCs may consist of silver, nickel, copper, etc., despite the fact that these metals are dispersive and absorptive in these frequency ranges [4].

MPCs are almost all fabricated as a combination of dielectric and metallic nanolayers or spheres in the form of one-, two-, and three-dimensional systems. For example, Scalora *et al.* [5] have investigated numerically the transmission of light passing through a one-dimensional MPC composed of a stack of alternating layers of silver (metal) and MgF_2 (dielectric). Their results showed that the structure remains transparent over a tunable range of frequencies, including the ultraviolet, visible, or infrared frequency range. Wang *et al.* [6] have theoretically studied the optical properties of a three-dimensional (3-D) self-assembled MPC consisting of spherical metal nanoparticles. For example, for silver spheres their band-structure calculations showed the formation of PBGs within the near-infrared to optical regime, even when absorption is taken into account. Kuo *et al.* [7] fabricated opaline gold photonic crystals possessing complete PBGs in the optical regime. Chang *et al.* [8] constructed a five-layer modified-woodpile 3-D MPC structure composed of gold, immersed in a dielectric material known as hydrogen silsesquioxane (HSQ) that exhibits characteristics of a 3-D complete PBG extending from near-infrared down to visible wavelengths at around 650 nm. Yang *et al.* [4] have fabricated a 3-D all-copper photonic crystal with a feature size of 0.20 μm by using electron-beam lithography with the photoresist of

HSQ, which can open a photonic band edge located at a wavelength of around 0.80 μm in normal incidence.

Confining and releasing light near the nanosized active medium such as dye molecules, impurity atoms, and QDs embedded in photonic crystals is one of the most important steps leading toward the development of optical switches [9] and optical transistors [10]. The control of confined light can be achieved using photonic crystals possessing tunable PBGs, by applying a coherent control energy [11]. It is also possible to control the PBGs of MPCs by changing the metallic dielectric function. For instance, the presence of a static magnetic field can greatly change the dielectric response of a free electron in the metal [12] or change the plasma energy by altering the surface charge density on each metallic particle [13,14].

Considerable effort has been devoted to the investigation of the quantum optics of MPCs doped with an active medium. For example, Kaso and John [15] have demonstrated the occurrence of nonlinear Bloch waves in MPCs when 5-nm-diameter PbS close-packed QDs fill the void regions. Singh [16] has studied the effect of plasmas on the bound photon modes in metallic photonic nanowires. Yannopapas *et al.* [17] have investigated the electromagnetically induced transparency when light is absorbed by a two-dimensional lattice of metallic (gold) spherical nanoparticles mounted on an asymmetric dielectric (indium-tin-oxide) waveguide.

Recently we have studied the quantum optics of four-level quantum dots doped in metallic photonic crystals [18]. A probe field was applied between the first excited state and higher excited states to study the absorption coefficient of the system in its steady-state configuration. It was considered that the first excited state decayed to the ground state. The density matrix method was used to calculate the absorption coefficient of the system. It was found that the height of the absorption peak can be controlled by changing the transition energy between the ground state and the first excited state.

In this research paper, we have considered a 3-D MPC doped with an ensemble of three-level QDs of V-configuration, as shown in Fig. 1. These particles consist of two upper levels, $|b\rangle$ and $|c\rangle$, and a ground state $|a\rangle$. We consider that spontaneous emission is allowed from the excited states (upper levels) to the ground state, whereas the $|c\rangle \leftrightarrow |b\rangle$ transition is inhibited in the electric dipole approximation. Quantum interference between spontaneous emission pathways from the transitions $|c\rangle \rightarrow |a\rangle$ and $|b\rangle \rightarrow |a\rangle$ is also considered. This reflects the fact that spontaneous emission from one excited level to the ground state can drive the other excited level, and vice versa, because of the quantum coherence between the two excited levels [19]. Quantum interference of spontaneous emission can lead to many remarkable phenomena such as coherent population trapping, lasing without inversion, optical transparency with slow light, and so on. For example, recently Gerardot *et al.* [20] have observed dressed states and quantum interference effects in a strongly driven three-level InAs/GaAs QDs ladder system embedded in a charge-tunable heterostructure. Huang *et al.* [21] purposed the optical amplification of probe field by using the induced electronic quantum interference in a pump-laser-driven three-level semiconductor quantum well without the population inversion. These achieved results have promising applications in quantum information processing and nonlinear optical devices.

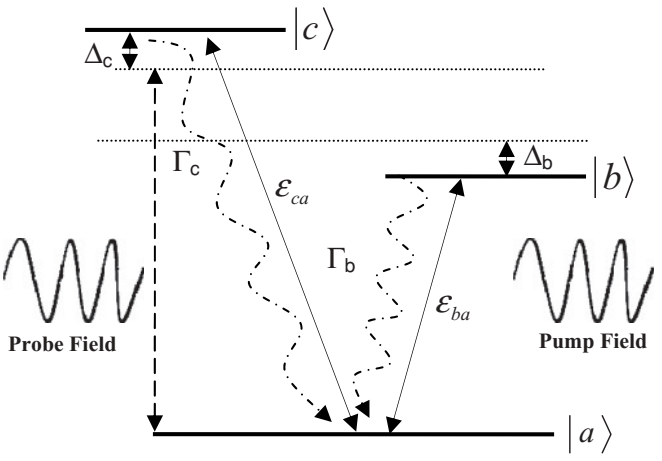

FIG. 1. Three-level QD in the V-configuration with two upper levels ($|c\rangle$ and $|b\rangle$) and ground state $|a\rangle$. Here we consider that the upper levels have energies that are very close to one another. The strong pump field of frequency ε_b is coupled to the ground sate $|a\rangle$ and the excited state $|b\rangle$, while the weak probe field of frequency ε_c is coupled to the ground sate $|a\rangle$ and the excited state state $|c\rangle$. Here ε_{ca} and ε_{ba} are the transition energies, respectively, while Γ_b and Γ_c are the decay rates from the exited states to ground state. The parameters $\Delta_c = (\varepsilon_{ca} - \varepsilon)/\hbar$ and $\Delta_b = (\varepsilon - \varepsilon_{ba})/\hbar$ are the detuning of the atomic transitions.

Here we study two different field configurations of QDs, as has been used in atomic vapors [22]. In the first configuration the exited energy levels are very close to one another, and the system is driven by a single probe laser field that is coupled with two transition energies simultaneously. This weak field facilitates the study of the absorption profile of the QDs. These conditions can be achieved by using a double quantum well system such as coupled $GaAs/Al_xGa_{1-x}As$ [23].

In the second configuration, the system is driven by a weak probe and strong pump field. It is considered that the QDs are interacting with each other via DDI, and also with the photonic crystal, which acts as a reservoir [24]. The density matrix method has been used to calculate the absorption coefficient and population density.

For the first configuration it is found that the system can be switched between transparent and absorption states by changing the plasma energy of the metallic spheres. In this case we have also calculated the time development of the absorption as the system approaches a steady state. For the second configuration it is found that the absorption coefficient peak splits into two peaks, and also the system can be switched from the absorption state to the gain state.

II. DENSITY MATRIX METHOD

We have considered that our MPC is fabricated from metallic spheres which are arranged in a periodic structure and embedded within a background dielectric material [3]. This dielectric background material can be taken as an ordinary dielectric material such as MgF_2 [5], Stycast, or Teflon [3], which have constant refractive indices. Here we take metallic spheres made of silver, as in [25]. The lattice constant of the crystal and radii of the spheres are taken as L and r_s, respectively, while the refractive index of the dielectric

background material is denoted as n_b. The refractive index of a metal, n_m, is energy dependent and is written as [26]

$$n_m(\varepsilon_k) = \sqrt{\left(1 - \frac{\varepsilon_p^2}{\varepsilon_k^2}\right) + \frac{\hbar\varepsilon_p^2}{\varepsilon_k^3\tau}i}, \tag{1}$$

where ε_k, ε_p, and τ are the energy of the incident electromagnetic (EM) wave, the plasma energy, and the relaxation time of the conduction-band electrons, respectively. The plasma energy is defined by $\varepsilon_p^2 = \hbar^2 N e^2/\varepsilon_0 m_{\text{eff}}$, where N is the electron density, m_{eff} is the effective mass of the electron, e is the electron charge, and ε_0 is the permittivity of the free space.

From Eq. (1), it is seen that when the energy of the incident light approaches the plasma energy, the real part of the dielectric function becomes infinitesimally small. This would imply that regardless of the magnitude of the dielectric constant of the background medium, the contrast is large enough to meet the requirement for the creation of a complete PBG. If we choose a proper metal which satisfies $\varepsilon_k\tau/\hbar \neq 1$ for large values of ε_p (in the range of visible light), the imaginary part of the dielectric function becomes small, and therefore the absorption can be negligible. Among all metals, only silver, copper, and gold would fulfill this criterion, since they have plasma energies within the optical regime due to d-electron band resonance as well as relaxation times on the order of a few tens of femtoseconds [7]. The range of light energy can also be less than the plasma energy when the real part of the dielectric function becomes negative. In this case, the radius of the metallic spheres can be chosen close to or smaller than the relevant skin depth of the corresponding metal, so that an EM wave in the visible energy range can be transmitted by tunneling through the structure [3,5].

Kee *et al.* [12] have shown that the refractive index of metallic nanolayers is modified in the presence of a large static magnetic field as

$$n_m(\varepsilon_k) = \sqrt{1 - \frac{\varepsilon_{pm}^2}{\varepsilon_k^2}}, \tag{2}$$

where

$$\varepsilon_{pm} = \frac{\varepsilon_p}{(1 \mp \hbar H_{\text{ext}}/8\pi\varepsilon_0 c m_{\text{eff}}\varepsilon_k)}. \tag{3}$$

In Eq. (3), the plus (minus) sign refers to left (right) circularly polarized EM waves, c is the speed of light in a vacuum, and H_{ext} is the magnitude of the external static magnetic field in cgs units. J. Rostalski *et al.* have also shown that that an excess charge on the surface of a metal nanoparticle would affect its plasma energy. Extra charge on the nanoparticles can be induced by friction, photoemission, and ion adhesion or bombardment. For example, in [14], the modified plasma energy for a spherical silver cluster is obtained as

$$\varepsilon_{pc}(n) = \varepsilon_{pc}(n_0)\sqrt{\frac{n_0 + n}{n_0}}, \tag{4}$$

where n_0 is the number of atoms in a metallic sphere, corresponding to the number of free electrons, and n is the number of excess electrons. This means that the plasma energy is increased by stationary surface charge on the uncharged sphere.

We consider that the MPC is doped with an ensemble of three-level QDs, as shown in Fig. 1. The QDs are interacting with the metallic crystal, which is acting as a reservoir. The electronic $|b\rangle \leftrightarrow |a\rangle$ and $|c\rangle \leftrightarrow |a\rangle$ transitions are interacting via electron-photon interaction in the dipole and rotating wave approximations. These electronic transitions induce a dipole moment in the QDs, and therefore these QDs are also interacting with each other through DDI [24]. The interaction Hamiltonian of the system is written as

$$H = -\sum_{i=b,c}\left[\int_C \frac{d\varepsilon_k}{2\pi}\sqrt{\gamma_0}Z_{ia}(\varepsilon_k)p(\varepsilon_k)\sigma_{ai}^{+} + \Lambda_{ia}\sigma_{ai}^{+} + \text{H.c.}\right], \tag{5}$$

where H.c. stands for the Hermitian conjugate. The first and second terms are the electron-photon interaction and the DDI, respectively. The term $\sigma_{ai}^{+} = |i\rangle\langle a|$ is called the electron raising operator, where $i = b$ or c, while $p(\varepsilon_k)$ is the photon annihilation operator. The integration contour C consists of two intervals due to the PBG of the MPC, which are $-\infty < \varepsilon_k \leqslant \varepsilon_l$ and $\varepsilon_u < \varepsilon_k \leqslant \infty$ [27]. The quantities ε_l and ε_u are the lower and upper edges of the PBG, respectively, while γ_0 is the vacuum decay rate and is defined in [28]. The function $Z(\varepsilon_k)$ is called the form factor and is obtained for the metallic crystal as [29]

$$Z(\varepsilon_k) = \left[\frac{2\pi^2 c^2\hbar^2 D(\varepsilon_k)}{\varepsilon_k^2}\right]^{1/2}, \tag{6}$$

where $D(\varepsilon_k)$, the density of states (DOS) of photons in the MPC, is written as [30]

$$D(\varepsilon_k) = \frac{\varepsilon_k^2\{\kappa[\cos(\varepsilon_k\theta_+) - \cos(\varepsilon_k\theta_-)] + \kappa_+\theta_+\sin(\varepsilon_k\theta_+) - \kappa_-\theta_-\sin(\varepsilon_k\theta_-)\}}{8\pi^2\hbar^2 c^2 L\sqrt{1 - F^2(\varepsilon_k)}}. \tag{7}$$

In Eq. (7), $L = 2r_s + 2b$ is the lattice constant and $F(\varepsilon_k)$ is obtained as

$$F(\varepsilon_k) = \sum_{\pm}\left[\pm\left(\frac{[n_m(\varepsilon_k) \pm n_b]^2}{4n_m(\varepsilon_k)n_b}\right) \times \cos\left(\frac{2\varepsilon_k[n_m(\varepsilon_k)r_s \pm n_b b]}{\hbar c}\right)\right]. \tag{8}$$

The other parameters in Eq. (7) are defined as

$$\kappa = \left(\frac{\varepsilon_p^2}{\varepsilon_k^2}\right)\left[\frac{1}{n_b\left(1 - \varepsilon_p^2/\varepsilon_k^2\right)^{1/2}} - \frac{1}{n_m\left(1 - \varepsilon_p^2/\varepsilon_k^2\right)^{1/2}}\right], \tag{9}$$

$$\kappa_{\pm} = \left[\frac{1}{n_b}\left(1 - \varepsilon_p^2/\varepsilon_k^2\right)^{1/2} - n_b\left(1 - \varepsilon_p^2/\varepsilon_k^2\right)^{1/2} \pm 2\right], \tag{10}$$

$$\theta_{\pm} = \frac{1}{\hbar c}\left[a\left(1-\varepsilon_p^2/\varepsilon_k^2\right)^{-1/2} \pm n_b b\right]. \tag{11}$$

Note that the DOS has singularity at the band edges where $F(\varepsilon_k) = 1$. In Eq. (5), Λ_{ia} is the DDI parameter defined as [24]

$$\Lambda_{ia} = \sum_{j=b,c i\neq j} [C_{ia}\rho_{ia} + C_{ij}\rho_{ja}], \tag{12}$$

where ρ_{ia} and ρ_{ja} are the density matrix elements associated with the transitions $|i\rangle \leftrightarrow |a\rangle$ and $|j\rangle \leftrightarrow |a\rangle$, respectively. The parameters C_{ia} and C_{ij} are the DDI coupling constants, which measure the strength of the DDI interaction. They are obtained as

$$C_{ba} = \left(\frac{N_0}{3\hbar\varepsilon_0}\right)\mu_{ba}, \quad C_{ca} = \left(\frac{N_0}{3\hbar\varepsilon_0}\right)\mu_{ca}^2, \quad C_{cb} = \left(\frac{N_0}{3\hbar\varepsilon_0}\right)\vec{\mu}_{ba}\cdot\vec{\mu}_{ca}, \tag{13}$$

where N_0 is the concentration of the QDs and μ_{ba} and μ_{ca} are electric dipole moments induced by the transitions $|b\rangle \leftrightarrow |a\rangle$ and $|c\rangle \leftrightarrow |a\rangle$, respectively.

The density matrices are calculated using the density matrix method developed in Ref. [31]. Using the interaction Hamiltonian given in Eq. (5), one can obtain the following expressions for the density matrices of a three-level energy system driven by two external laser fields, with the system prepared in such a way that initially the QDs are in the ground state $|a\rangle$:

$$\begin{aligned}\frac{d\rho_{ba}}{d\tau} &= -[d_{ba} + i\alpha_{ba}(\rho_{bb}-\rho_{aa}) + i\alpha_{cb}\rho_{bc}]\rho_{ba} \\ &\quad - i(\Omega_c + \alpha_{ca}\rho_{ca})\rho_{bc} - i\Omega_b(\rho_{bb}-\rho_{aa}) \\ &\quad - \frac{P_0\sqrt{\Gamma_b\Gamma_c}}{\Gamma_0}[1 + i\sqrt{\alpha_{ba}\alpha_{ca}}(\rho_{bb}-\rho_{aa})]\rho_{ca}, \end{aligned} \tag{14}$$

$$\begin{aligned}\frac{d\rho_{ca}}{d\tau} &= -[d_{ca} + i\alpha_{ca}(\rho_{cc}-\rho_{aa}) + i\alpha_{cb}\rho_{cb}]\rho_{ca} \\ &\quad - i(\Omega_b + \alpha_{ba}\rho_{ba})\rho_{cb} - i\Omega_c(\rho_{cc}-\rho_{aa}) \\ &\quad - \frac{P_0\sqrt{\Gamma_b\Gamma_c}}{\Gamma_0}[1 + i\sqrt{\alpha_{ba}\alpha_{ca}}(\rho_{cc}-\rho_{aa})]\rho_{ba}, \end{aligned} \tag{15}$$

$$\begin{aligned}\frac{d\rho_{cb}}{d\tau} &= -d_{cb}\rho_{cb} + i\Omega_c\rho_{ab} - i\Omega_b\rho_{ca} - \frac{P_0\sqrt{\Gamma_b\Gamma_c}}{\Gamma_0}(\rho_{cc}+\rho_{bb}) \\ &\quad - i(\alpha_{ba}-\alpha_{ca})\rho_{ca}\rho_{ab} + i\alpha_{cb}(|\rho_{ba}|^2 - |\rho_{ca}|^2), \end{aligned} \tag{16}$$

$$\begin{aligned}\frac{d\rho_{cc}}{d\tau} &= -2\frac{\Gamma_c}{\Gamma_0}\rho_{cc} - i\Omega_c(\rho_{ca}-\rho_{ac}) - \frac{P_0\sqrt{\Gamma_b\Gamma_c}}{\Gamma_0}(\rho_{cb}+\rho_{bc}) \\ &\quad + i\alpha_{cb}(\rho_{ba}\rho_{ac} - \rho_{ab}\rho_{ca}), \end{aligned} \tag{17}$$

$$\begin{aligned}\frac{d\rho_{bb}}{d\tau} &= -2\frac{\Gamma_b}{\Gamma_0}\rho_{bb} - i\Omega_b(\rho_{ba}-\rho_{ab}) - \frac{P_0\sqrt{\Gamma_b\Gamma_c}}{\Gamma_0}(\rho_{cb}+\rho_{bc}) \\ &\quad + i\alpha_{cb}(\rho_{ab}\rho_{ca} - \rho_{ba}\rho_{ac}), \end{aligned} \tag{18}$$

where

$$d_{ca} = \frac{2}{\Gamma_0}\left(\frac{\Gamma_c}{2} + i\Delta_c\right), \quad d_{ba} = \frac{2}{\Gamma_0}\left(\frac{\Gamma_b}{2} + i\Delta_b\right), \quad d_{cb} = \frac{2}{\Gamma_0}\left[\frac{\Gamma_c+\Gamma_b}{2} + i(\Delta_c-\Delta_b)\right]. \tag{19}$$

Here Γ_b and Γ_c denote the decay rates (linewidths) related to the $|b\rangle \leftrightarrow |a\rangle$ and $|c\rangle \leftrightarrow |a\rangle$ transitions due to coupling of the electron-photon interaction, respectively, and are obtained as

$$\Gamma_b(\varepsilon_{ba}) = \gamma_0 Z(\varepsilon_{ba})^2, \quad \Gamma_c(\varepsilon_{ca}) = \gamma_0 Z(\varepsilon_{ca})^2. \tag{20}$$

The quantities ε_{ba} and ε_{ca} are the transition energies corresponding to the $|b\rangle \leftrightarrow |a\rangle$ and $|c\rangle \leftrightarrow |a\rangle$ transitions, respectively. In Eq. (19), $\Delta_c = (\varepsilon_{ca}-\varepsilon)/\hbar$ and $\Delta_b = (\varepsilon-\varepsilon_{ba})/\hbar$ are the detuning parameters for each transition energy. In our calculations, all energies have been normalized with respect to $\Gamma_0(\varepsilon_m)/2$, where ε_m lies far away from the PBG of the MPC. By using this definition the normalized time is taken: $\tau = (\Gamma_0/2)t$. The effect of quantum interference resulting from the cross coupling between the $|b\rangle \leftrightarrow |a\rangle$ and $|c\rangle \leftrightarrow |a\rangle$ transitions is given by $P_0 = \vec{\mu}_{ca}\cdot\vec{\mu}_{ba}/\mu_{ca}\mu_{ba}$ [19]. Optimal quantum interference is achieved when the dipole moments are parallel. In Eqs. (14)–(18), $\Omega_b = \vec{\mu}_{ba}\cdot\vec{E}_b/\hbar\Gamma_0$ and $\Omega_c = \vec{\mu}_{ca}\cdot\vec{E}_c/\hbar\Gamma_0$ are the normalized Rabi frequencies of the transitions $|b\rangle \leftrightarrow |a\rangle$ and $|c\rangle \leftrightarrow |a\rangle$, respectively, where E_b and E_c are the slowly varying amplitudes of the two laser beams. The normalized DDI parameters are $\alpha_{ca} = 2C_{ca}/\Gamma_0$, $\alpha_{ba} = 2C_{ba}/\Gamma_0$, and $\alpha_{cb} = 2C_{cb}/\Gamma_0$. Note that population conservation requires that $\rho_{aa}(t) + \rho_{bb}(t) + \rho_{cc}(t) = 1$ and also $\rho_{ij} = \rho_{ji}^*$.

In the first configuration we assume that the two upper excited levels of the QDs ($|b\rangle$ and $|c\rangle$) are close to one another, so they are almost degenerate. Here the pump field is absent, and the transitions $|b\rangle \leftrightarrow |a\rangle$ and $|c\rangle \leftrightarrow |a\rangle$ are simultaneously driven by a weak tunable probe field of energy ε_c.

For this configuration, the absorption due to the $|b\rangle \leftrightarrow |a\rangle$ and $|c\rangle \leftrightarrow |a\rangle$ transitions in the presence of the applied probe field is written as [28]

$$\alpha(t) = \alpha_0 \mathrm{Im}[\rho_{ab}(t) + \rho_{ac}(t)], \tag{21}$$

where α_0 is obtained as

$$\alpha_0 = \frac{N_0\mu^2\varepsilon_c}{\varepsilon\Omega_c\hbar c\Gamma_0}. \tag{22}$$

Here ε is the dielectric constant of the medium, μ is the induced dipole moment ($\mu = \mu_{ba} = \mu_{ca}$), and ρ_{ab} and ρ_{ac} are the density matrix elements for transitions $|b\rangle \leftrightarrow |a\rangle$ and $|c\rangle \leftrightarrow |a\rangle$, respectively. In this case the normalized detuning parameter represents probe laser detuning from the resonance with the center of the excited levels [i.e., $\delta_k = (\Delta_b + \Delta_c)/\Gamma_0$].

For this configuration we have obtained the following analytical expression for the absorption coefficient in the linear response approximation of the Rabi frequency by using a very low driving field:

$$\frac{\alpha}{\alpha_0} = \frac{[1 + a_1(\alpha_{cb}-\alpha_{ca}) + a_2(\alpha_{ca}-\alpha_{cb})](a_3+a_4) + [a_4(\alpha_{ca}-\alpha_{cb}) - a_3(\alpha_{ba}+\alpha_{cb}) + 1](a_2+a_1)}{(1-a_1\alpha_{ca}-a_2\alpha_{cb})(1-a_3\alpha_{ba}-a_4\alpha_{cb}) - (a_4\alpha_{ca}+a_3\alpha_{cb})(a_2\alpha_{ba}+a_1\alpha_{cb})}, \tag{23}$$

$$a_1 = i\left[\frac{d_{ba}d_{cb}(\rho^0_{aa}-\rho^0_{cc}) - P^2(\rho^0_{cc}+\rho^0_{bb})}{d_{cb}(d_{ba}d_{ca}-P^2)}\right], \quad (24)$$

$$a_2 = iP\left[\frac{d_{ba}(\rho^0_{cc}+\rho^0_{bb}) - d_{cb}(\rho^0_{aa}-\rho^0_{bb})}{d_{cb}(d_{ba}d_{ca}-P^2)}\right], \quad (25)$$

$$a_3 = i\left[\frac{d_{cb}d_{ca}(\rho^0_{aa}-\rho^0_{bb}) - P^2(\rho^0_{cc}+\rho^0_{bb})}{d_{cb}(d_{ba}d_{ca}-P^2)}\right], \quad (26)$$

$$a_4 = -iP\left[\frac{d_{cb}(\rho^0_{aa}-\rho^0_{bb}) + d_{ca}(\rho^0_{cc}+\rho^0_{bb})}{d_{cb}(d_{ba}d_{ca}-P^2)}\right]. \quad (27)$$

Throughout Eqs. (23)–(27), ρ^0_{ij} denotes the elements of the density matrix at $t=0$ and $P = P_0\sqrt{\Gamma_b\Gamma_c}/\Gamma_0$ represents the quantum interference.

In the second configuration, a probe laser field of normalized Rabi frequency Ω_{0c} sweeps the $|c\rangle \leftrightarrow |a\rangle$ transition in order to study the absorption coefficient of the QDs. Here the $|b\rangle \leftrightarrow |a\rangle$ transition is driven by a strong control laser field of normalized Rabi frequency Ω_{0b}, which manipulates the absorption coefficient. This configuration is one the most famous utilized models that study quantum coherence and interference effects in three- or multilevel atoms [32]. In this case the absorption coefficient is obtained as [33]

$$\alpha = \alpha_0\{\mathrm{Im}[\rho_{ac}(\Omega_c) - \rho_{ac}(\Omega_c = 0)]\}, \quad (28)$$

In this configuration the Rabi frequencies Ω_b and Ω_c appearing in Eqs. (14)–(18) are replaced by $\bar{\Omega}_b = \Omega_b\sqrt{1-P_0^2}$ and $\bar{\Omega}_c = \Omega_c\sqrt{1-P_0^2}$, respectively. In this configuration, we are not able to obtain the analytical expression for the absorption coefficient. Here the normalized detuning parameter represents the difference between the probe laser resonance and the excited level $|c\rangle$ (i.e., $\delta_k = 2\Delta_c/\Gamma_0$).

III. RESULTS AND DISCUSSION

Our main focus in this section is to vary the plasma energy and then observe the effect this has on the absorption coefficient profile for both QD-field configurations. We have considered that our MPC is made from silver spheres embedded in MgF_2 ($n_b = 1.5$) [34]. The radius of the metallic spheres and lattice constant of the PC in reduced units are chosen as $r_s = 0.25\hbar c/\varepsilon_p$ and $L = 10.5\hbar c/\varepsilon_p$, respectively [35]. The energies of the lower and upper photonic band edges are calculated as $\varepsilon_l = 1.81$ eV and $\varepsilon_u = 2.48$ eV, respectively, for silver spheres with $\varepsilon_p = 9$ eV [6]. Note that the PBG lies in the optical energy range, which shows that our theoretical model is in good agreement with recent experimental results [36].

The physical parameters appearing in the absorption coefficient expression are taken from Ref. [22]. The linewidths Γ_b and Γ_c are calculated by using Eq. (20) for the resonance energies ε_{ba} and ε_{ca}. For the first configuration, the normalized absorption coefficient (α/α_0) is plotted in Fig. 2. as a function of the normalized detuning parameter $[\delta_k = (\Delta_b + \Delta_c)/\Gamma_0]$, using the analytical expression obtained in Eq. (23). The energy levels $\varepsilon_{ba} = 2.6$ eV and $\varepsilon_{ca} = 2.6001$ eV are located very close to each other, as the energy difference between $|b\rangle$ and $|c\rangle$ is taken as $\varepsilon_{cb} = 0.1$ meV. In our calculation the normalized energy factor is defined as $\Gamma_0 = 1.5751\gamma_0$,

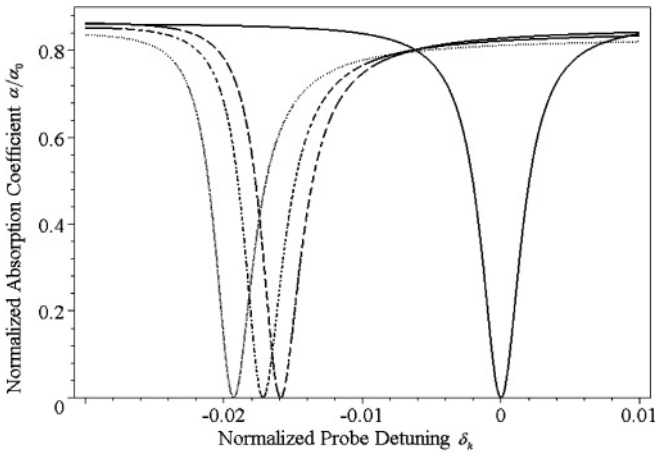

FIG. 2. Steady-state results for the normalized absorption spectrum (α/α_0), given in arbitrary units, as a function of the normalized probe field detuning (δ_k), which given in Eq. (23). The solid curve corresponds to $\alpha = 0$ and $\varepsilon_p = 9$ eV. For the dotted, dash-dotted, and dashed curves we have $\alpha = 0.1$, while the plasma energy is varied as $\varepsilon_p = 9$ eV (dotted curve), 8.97 eV (dash-dotted curve), and 8.95 eV (dashed curve).

which gives a decay rate with energy $\varepsilon_m = 2.92$ eV. The quantity γ_0 is taken as $\gamma_0 = 1$ meV/$\hbar$, from Ref. [28]. All DDI parameters are considered equal (i.e., $\alpha_{ca} = \alpha_{cb} = \alpha_{cb} = \alpha$), and the maximum quantum interference strength is applied (i.e., $P_0 = 1$).

In Fig. 2, the solid and dotted curves show the normalized absorption coefficients for the DDI parameters $\alpha = 0$ and $\alpha = 0.1$, respectively, while the plasma energy in both cases is taken as $\varepsilon_p = 9$ eV. We note that the absorption spectrum has one sharp dip and two peaks. However, the two peaks are not shown in Fig. 2 because the detuning parameter is taken to lie very close to the dip. The dip in absorption corresponds to a transparent resonance,and is due to the cancellation of the spontaneous emission through quantum interference. Note that in the presence of DDI the sharp dip in the absorption profile shifts to the left side of the zero detuning $\delta_k = -0.019$, as indicated by the dotted curve in Fig. 2. This shift in the dip is due to the presence of DDI, which causes a change in the detuning parameter, as the energy difference between levels $|b\rangle$ and $|c\rangle$ changes [see Eq. (5)].

Interesting results are obtained when the plasma energy of the MPC is changed while considering the DDI ($\alpha = 0.1$). The dotted, dash-dotted, and dashed curves are plotted for $\varepsilon_p = 9$ eV, $\varepsilon_p = 8.97$ eV, and $\varepsilon_p = 8.95$ eV, respectively. When the plasma energy decreases, the dip shifts to new locations at $\delta_k = -0.017$ and $\delta_k = -0.016$. Consequently, the transparency at $\delta_k = -0.019$ disappears and is replaced with strong absorption. This phenomenon occurs because the locations of band edges of the MPC changes when the plasma energy is modified. This change in the PBG affects the linewidths Γ_b and Γ_c through the form factor [see Eqs. (6) and (20)]. In summary, these results demonstrate that the system can be switched from an absorbing state to a transparent state by changing the plasma energy in the presence of DDI.

To understand the physical behavior of the system at $\delta_k = -0.019$ due to the plasma energy, we have studied

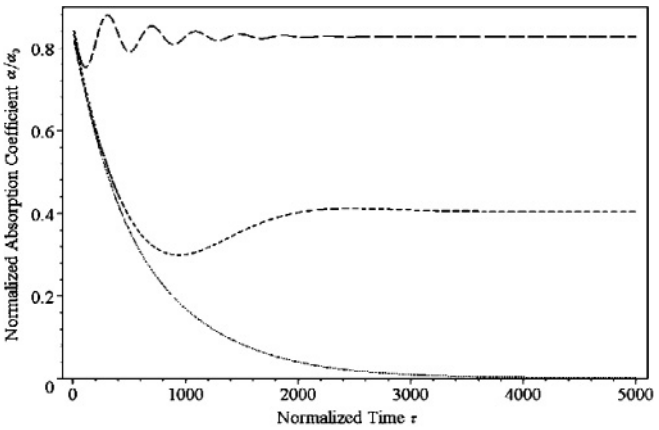

FIG. 3. Numerical plots of the time evolution of the normalized absorption coefficient versus normalized time τ for plasma frequency $\varepsilon_p = 9$ eV (dotted curve), $\varepsilon_p = 8.97$ eV (dashed curve), and $\varepsilon_p = 8.95$ eV (long dashed curve). Here $\Gamma_0(2.92\text{ eV}) = 1.5751\gamma_0$ for $\varepsilon_{bc} = 0.1$ meV, $\Omega_a = \Omega_b = 0.01$, and $P_0 = 1$.

the time evolution of the absorption spectrum. Here, the differential equations for the density matrix elements given in Eqs. (14)–(18) in the presence of DDI for a weak laser probe field ($\Omega_c = \Omega_b = 0.01$) are solved numerically. We have used the DVERK78 method (seventh- to eighth-order continuous Runge-Kutta) provided by MAPLE. Our results show that the DVERK78 method has a rather higher precision in comparison to other available methods. As an initial condition, we assume that $\rho_{aa}^{(0)} = 1$, $\rho_{bb}^{(0)} = \rho_{cc}^{(0)} = 0$, and $\rho_{ij}^{(0)} = 0$. This result is plotted in Fig. 3, where the dotted, dashed, and long-dashed curves are plotted for plasma energies $\varepsilon_p = 9$ eV, $\varepsilon_p = 8.97$ eV, and $\varepsilon_p = 8.95$ eV, respectively.

Our calculations show that, for $\varepsilon_p = 8.95$ eV, the absorption profile exhibits oscillations and eventually reaches a steady state. However, when we change the plasma energy to $\varepsilon_p = 9$ eV, the oscillatory behavior of the absorption profile disappears, and the system becomes transparent, reaching its steady state exponentially. Note that the achieved results have a reasonable explanation based on the derived theory associated with the temporal behavior of the absorption profile. It is well known that the number of oscillations during the temporal evolution of quantum coherence is proportional to the value of the decay rate for related energy transitions [37]. As the linewidths increase, the number of oscillations decreases.

To show the variation of the linewidths (Γ_b and Γ_c) as a function of plasma energy, the form factor squared $[Z^2(\varepsilon_p)]$ is plotted in Fig. 4 for different photon energies (ε_k), lying just above the upper photonic band edge. In this figure, the solid, dashed, and dash-dotted curves correspond to photon energies of $\varepsilon_k = 2.6$ eV, $\varepsilon_k = 2.61$ eV, and $\varepsilon_k = 2.62$ eV, respectively. From these results, it is seen that the linewidths increase when the plasma energy increases. Note that in Fig. 4, the lattice constant of the MPC and the radius of the metallic spheres are given as functions of the plasma energy, which is done in order to simplify our numerical simulations. For the range of plasma energies considered, the variation in these parameters is negligibly small and thus can be ignored.

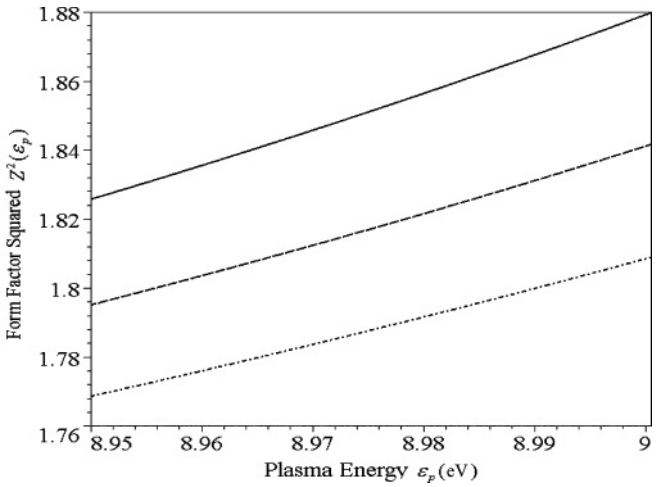

FIG. 4. Plot of the form factor squared $[Z^2(\varepsilon_p)]$ just above the upper photonic band edge versus the plasma energy for a MPC with $n_m(\varepsilon_k) = \sqrt{1 - \varepsilon_p^2/\varepsilon_p^2}$, $n_b = 1.5$, $r_s = 0.25\hbar c/\varepsilon_p$, and $L = 10.5\hbar c/\varepsilon_p$, for $\varepsilon_k = 2.6$ eV (solid curve), $\varepsilon_k = 2.61$ eV (dashed curve), and $\varepsilon_k = 2.62$ eV (dash-dotted curve).

We have again calculated the absorption coefficient using Eqs. (14)–(20) to investigate the accuracy of the derived analytical expression for the first configuration. We found that there is a good agreement between analytical and exact calculations for small values of DDI parameters. These results are not plotted because they give the same curves as in Fig. 2. This means that the analytical expression obtained in this paper gives excellent results for small values of DDI parameters, and it can be used by experimentalists to compare their results with the present theory. However, the analytical expression does not agree with the exact expression for large values of α. In Fig. 5, the dashed and solid curves show results from the numerical calculation and analytical expression, respectively. As one can

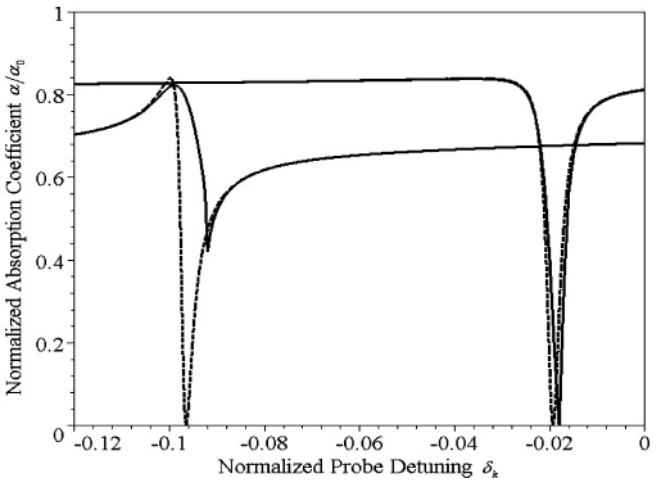

FIG. 5. Steady-state results for normalized absorption spectrum (α/α_0) in arbitrary units as a function of the normalized probe field detuning (δ_k). Here the dashed curves show the results obtained from the derived analytical expression given in Eq. (23), while the solid curves are obtained by numerically solving Eqs. (14)–(20). Parameters for this figure are taken as $\varepsilon_p = 9$ eV, $\alpha = 0.1$, and $\alpha = 0.5$.

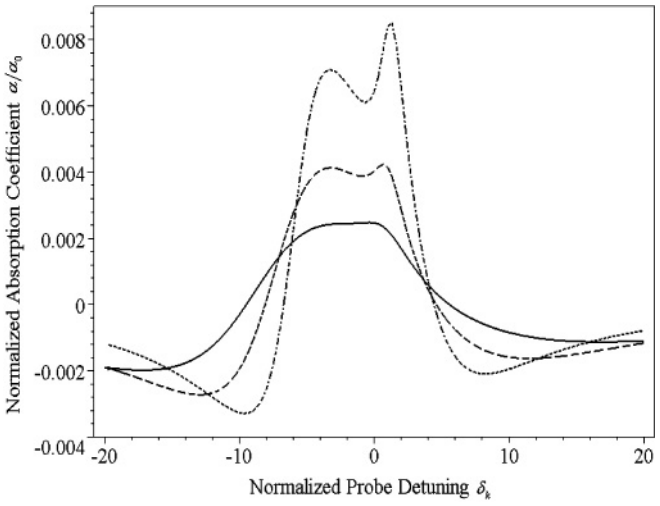

FIG. 6. Steady-state results for normalized absorption spectrum (α/α_0), in arbitrary units, as a function of the normalized probe field detuning ($\delta_k = 2\Delta_c/\Gamma_0$) for a fixed value of DDI parameter ($\alpha = 1$) and different plasma energies. The $|c\rangle \leftrightarrow |a\rangle$ transition decay rate $\Gamma_c(\varepsilon_{ac} = 2.4857$ eV) is $41.28\gamma_0$ for $\varepsilon_p = 9.00$ eV (solid curves), $23.33\gamma_0$ for $\varepsilon_p = 8.999$ eV (dashed curves), and $12.13\gamma_0$ for $\varepsilon_p = 8.995$ eV (dash-dotted curves). The $|b\rangle \leftrightarrow |a\rangle$ transition decay rate $\Gamma_b(\varepsilon_{ab} = 2.9$ eV) is $1.575\gamma_0$. The other parameters are $\Delta_b = 0$ (the pump laser field detuning), $P_0 = 0.99$ (quantum interference), $\Omega_c = 1$, and $\Omega_b = 20$ (normalized Rabi frequencies).

see for $\alpha = 0.1$, these curves are closely matched around $\delta_k = -0.02$. As the DDI parameter increases to $\alpha = 0.5$, both curves shift to the left but they are no longer closely matched.

For the second configuration the normalized absorption coefficient is calculated by numerically solving Eqs. (14)–(20), with the same set of initial conditions. The pump laser field is considered to be resonant with the $|b\rangle \leftrightarrow |a\rangle$ transition, (i.e., $\Delta_b = 0$). Let us first consider a situation when the resonance energy ε_{ac} for transition $|a\rangle \leftrightarrow |c\rangle$ lies near the band edge and the resonance energy ε_{ab} for transition $|a\rangle \leftrightarrow |b\rangle$ lies far away from the band edge. The resonance energies are are taken as $\varepsilon_{ac} = 2.4857$ eV and $\varepsilon_{ab} = 2.9$ eV. Note that in this configuration, the resonance energies are not close to each other. The normalized Rabi frequencies of the pump and probe fields are taken as $\Omega_c = 1$ and $\Omega_b = 20$. Here the strength of the quantum interference, P_0, is taken as 0.99 [22].

Figure 6 shows the steady state of the absorption profile versus the normalized probe laser detuning ($\delta_k = 2\Delta_c/\Gamma_0$), while considering the DDI ($\alpha = 1$). The solid, dashed, and dash-doted curves correspond to plasma energies of $\varepsilon_p = 9.00$ eV, $\varepsilon_p = 8.999$ eV, and $\varepsilon_p = 8.995$ eV. Note that the absorption coefficient has only one peak for $\varepsilon_p = 9.00$ eV, which splits into two peaks for plasma energies $\varepsilon_p = 8.999$ eV and $\varepsilon_p = 8.995$ eV. This splitting, which is well known as the induced Autler-Townes splitting [38], is due to the splitting of the ground state because of the presence of the strong pump field. This splitting disappears for $\varepsilon_p = 9.00$ eV because of the broadening of dressed states which are larger than the energy splitting. These results show that the system can be switched from one absorption peak to two by changing the plasma frequency. In Fig. 6, the DDI causes the observed asymmetry and the small amount of gain with inversion, which corresponds to the negative values of absorption.

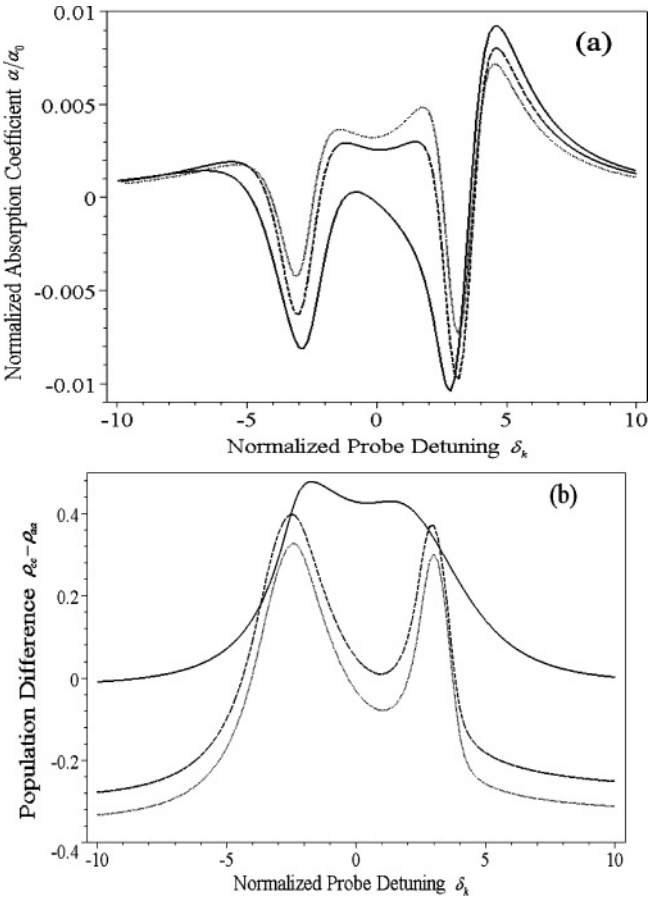

FIG. 7. (a) Steady-state results for normalized absorption spectrum (α/α_0) in arbitrary units and (b) population difference ($\rho_{cc} - \rho_{aa}$) as a function of the normalized probe field detuning ($\delta_k = 2\Delta_c\Gamma_0$) for a fixed and different value of DDI parameter and plasma energy, respectively. The $|b\rangle \leftrightarrow |a\rangle$ transition decay rate $\Gamma_b(\varepsilon_{ab} = 2.487$ eV) is $12.46\gamma_0$ for $\varepsilon_p = 9.00$ eV (solid curves), $4.90\gamma_0$ for $\varepsilon_p = 8.97$ eV (dashed curves), and $3.98\gamma_0$ for $\varepsilon_p = 8.95$ eV (dotted curves). The $|c\rangle \leftrightarrow |a\rangle$ transition decay rate $\Gamma_c(\varepsilon_{ac} = 2.9$ eV) is $1.575\gamma_0$. The other parameters are $\Delta_b = 0$ (the pump laser field detuning), $P_0 = 0.99$ (quantum interference), $\Omega_c = 1$, and $\Omega_b = 20$ (normalized Rabi frequencies).

Another remarkable result is shown in Fig. 7, when we consider a reverse situation where the resonance energy ε_{ac} for $|a\rangle \leftrightarrow |c\rangle$ lies far away from the band edge and the resonance energy ε_{ab} for transition $|a\rangle \leftrightarrow |b\rangle$ lies near the band edge. In this case the resonant energies are taken as $\varepsilon_{ac} = 2.9$ eV and $\varepsilon_{ab} = 2.487$ eV. As seen in Fig. 7(a), the peak in the absorption coefficient for $\varepsilon_p = 9.00$ eV (solid curve) is almost below zero, lying near the zero detuning parameter ($\delta_k = 0$). If we decrease ε_p, the solid peak moves above the zero line and starts splitting into two peaks due to the Autler-Townes splitting, as shown by the dashed and dotted curves. Thus, we find that the system changes from gain to absorption around the zero detuning parameter. This effect is also known as population inversion. To show the population inversion we have also plotted the population difference ($\rho_{cc} - \rho_{aa}$) in Fig. 7(b). One can see

clearly that for $\varepsilon_p = 8.97$ eV and $\varepsilon_p = 8.95$ eV, there is no population inversion near the zero detuning parameter. For $\varepsilon_p = 9.00$ eV, the curve moves to the positive region and population inversion occurs. This means that population inversion in the system can be achieved by changing the plasma energy.

The gain state in the system is due to the quantum coherences in the $|b\rangle \leftrightarrow |a\rangle$ and $|c\rangle \leftrightarrow |a\rangle$ transitions [i.e., $\mathrm{Im}(\rho_{ba})$ and $\mathrm{Im}(\rho_{ca})$] and quantum interference P [39]. When the plasma energy lies, for example, at $\varepsilon_p = 8.95$ eV, Γ_b is greater than Γ_c, and so the electrons in state $|b\rangle$ have a smaller lifetime than electrons in state $|c\rangle$. Due to quantum coherence, more electrons move from state $|b\rangle$ to state $|c\rangle$ via state $|a\rangle$ than the from state $|c\rangle$ to $|b\rangle$, but for this case we do not get $\rho_{cc} > \rho_{aa}$. However, when we change the plasma energy to $\varepsilon_p = 8.97$ eV, the linewidth for transition $|b\rangle \leftrightarrow |a\rangle$ (Γ_b) becomes very large compared to that for transition $|c\rangle \leftrightarrow |a\rangle$ (Γ_c). In this case a large number of electrons move from state $|b\rangle$ to $|c\rangle$ because the lifetime of state $|b\rangle$ is very small compared to the lifetime of state $|c\rangle$; thus we observe gain.

Finally, we comment on a possible switching nanoscale device made by using the physics of the present paper. We have found that three-level quantum dots doped in metallic photonic crystals can be switched from a transparent state to an absorbing state by changing the plasma energy. The plasma energy of metals can be changed by applying a pulsed magnetic field, as pointed out in Ref. [12]. By applying such a field, the photonic device formed from nanosize quantum dots doped in a metallic photonic crystal can be switched from the ON position to the OFF position. For example, with a certain plasma energy the system will be in its transparent state. Therefore, in this case the probe laser will propagate through the system, and the optical switch can be considered to be in an OFF position. On the other hand, due to the application of the pulsed magnetic field, the plasma energy can be changed in such a way so that the system switches to the absorbing state. Then the laser beam will be completely reflected by the system, and in this case the switch is ON.

IV. CONCLUSION

In this paper we have studied the effect of a changing plasma frequency on the absorption profile of quantum dots. We consider that the quantum dots are doped in a metallic photonic crystal fabricated from metallic spheres embedded in a background dielectric material. These quantum dots are considered as an ensemble of three-level energy systems, containing two excited states and a ground state. The quantum dots are interacting with each other via the dipole-dipole interaction, and they are coupled with plasma-photon modes present the system. We also consider quantum interference between the two decay channels from the excited levels to the ground state. We consider that a probe laser field is applied to the system in order to study the absorption coefficient for two possible field configurations. Absorption occurs due to the transitions from the ground state to an excited state, and it is calculated by using the density matrix method. In the first configuration, the probe field couples with the ground state and the two excited states, which have energies lying very close to one another. In the dipole approximation, the transition between excited states is forbidden. In this case it is found that the position of the transparent peak is moved, due to a slight change in the plasma energy. This means that the transparent state becomes an absorbing state. In the second configuration, a pump field couples with only one excited state, while the probe field couples to the other. In this case, we found that a peak in the absorption profile appears due to plasmon coupling, and this peak splits into two peaks when the plasma energy is decreased. This change in plasma energy can also take the system from the absorption region to the gain region. These are very interesting results and can be useful for developing nanoscale plasmonic devices.

ACKNOWLEDGMENTS

The authors are grateful to NSERC of Canada for financial support in the form of a research grant and to Mr. J. Cox for proofreading the paper.

[1] A. Moroz, Phys. Rev. Lett. **83**, 5274 (1999).
[2] R. Biswas, M. M. Sigalas, G. Subramania, and K. M. Ho, Phys. Rev. B **57**, 3701 (1998).
[3] E. R. Brown and O. B. McMahon, Appl. Phys. Lett. **67**, 2138 (1995).
[4] Y. L. Yang, F. J. Hou, S. C. Wu, W. H. Huang, M. C. Lai, and Y. T. Huang, Appl. Phys. Lett. **94**, 041122 (2009).
[5] M. Scalora, M. J. Bloemer, A. S. Pethel, J. P. Dowling, C. M. Bowden, and A. S. Manka, J. Appl. Phys. **83**, 2377 (1998).
[6] Z. Wang, C. T. Chan, W. Zhang, N. Ming, and P. Sheng, Phys. Rev. B **64**, 113108 (2001).
[7] C. Y. Kuo and S. Y. Lu, Appl. Phys. Lett. **92**, 121919 (2008).
[8] A. S. P. Chang, Y. S. Kim, M. Chen, Z. P. Yang, J. A. Bur, S. Y. Lin, and K. M. Ho, Opt. Express **15**, 8428 (2007).
[9] M. Florescu and S. John, Phys. Rev. A **64**, 033801 (2001).
[10] M. Florescu and S. John, Phys. Rev. A **69**, 053810 (2004).
[11] M. Woldeyohannes and S. John, Phys. Rev. A **60**, 5046 (1999).
[12] C. S. Kee, J. E. Kim, and H. Y. Park, Phys. Rev. E **57**, 2327 (1998).
[13] T. Ung, M. Giersig, D. Dunstan, and P. Mulvaney, Langmuir **13**, 1773 (1997).
[14] J. Rostalski and M. Quinten, Colloid Polym. Sci. **274**, 648 (1996).
[15] A. Kaso and S. John, Phys. Rev. A **76**, 053838 (2007).
[16] M. R. Singh, J. Appl. Phys. **106**, 063106 (2009).
[17] V. Yannopapas, E. Paspalakis, and N. V. Vitanov, Phys. Rev. B **80**, 035104 (2009).
[18] A. Hatef and M. Singh, Nanoscale Res. Lett. **5**, 464 (2010).
[19] E. Paspalakis, S. Q. Gong, and P. L. Knight, Opt. Commun. **152**, 293 (1998).
[20] B. D. Gerardot, D. Brunner, P. A. Dalgarno, K. Karrai, A. Badolato, P. M. Petroff, and R. J. Warburton, New J. Phys. **11**, 013028 (2009).

[21] D. Huang, P. M. Aising, D. A. Cardimona, and G. A. Gumbs, IEEE Trans. Nanotechnol. **7**, 151 (2008).
[22] O. G. Calderon, M. A. Anton, and F. Carreno, Eur. Phys. J. D **25**, 77 (2003).
[23] X. Hao, J. Li, X. Y. Lv, L. G. Si, and X. Yang, Phys. Lett. A **373**, 3827 (2009).
[24] M. R. Singh, Phys. Rev. A **75**, 043809 (2007).
[25] K. P. Velikov, W. L. Vos, A. Moroz, and A. Van Blaaderen, Phys. Rev. B **69**, 075108 (2004).
[26] G. Veronis, R. W. Dutton, and S. Fan, J. Appl. Phys. **97**, 1 (2005).
[27] I. Haque and M. R. Singh, J. Phys. Condens. Matter **19**, 156229 (2007).
[28] M. R. Singh, J. Mod. Opt. **56**, 758 (2009).
[29] V. I. Rupasov and M. Singh, Phys. Rev. A **56**, 898 (1997).
[30] M. R. Singh, Phys. Rev. A **79**, 013826 (2009).
[31] Z. Ficek and S. Swain, *Quantum Interference and Coherence: Theory and Experiments* (Springer, New York, 2005).
[32] P. Li, X. J. Ning, Q. Zhang, and J. Q. You, J. Phys. B **41**, 235401 (2008).
[33] J. C. Petch, C. H. Keitel, P. L. Knight, and J. P. Marangos, Phys. Rev. A **53**, 543 (1996).
[34] M. J. Keskinen, P. Loschialpo, D. Forester, and J. Schelleng, J. Appl. Phys. **88**, 5785 (2000).
[35] X. Xu, Y. Xi, D. Han, X. Liu, J. Zi, and Z. Zhu, Appl. Phys. Lett. **86**, 091112 (2005).
[36] V. Kamaev, C. Liu, A. L. Pokrovsky, C. Y. Li, A. L. Efros, and Z. Valy Vardeny, Proc. SPIE Int. Soc. Opt. Eng. **5927**, 592712 (2005).
[37] M. O. Scully and M. S. Zubairy, *Quantum Optics* (Cambridge University Press, Cambridge, UK, 1997), Chap. 7, pp. 241–244.
[38] I. Kenyon, *The Light Fantastic: A Modern Introduction to Classical and Quantum Optics* (Oxford University Press, New York, 2008), Chap. 17, pp. 537–538.
[39] S. Q. Gong, E. Paspalakis, and P. L. Knight, J. Mod. Opt. **45**, 12 (1998).